East European Journal of Physics. 3. 447-455 (2024)
DOI:10.26565/2312-4334-2024-3-54 ISSN 2312-4334

SCAPS-1D ANALYSIS OF NON-TOXIC LEAD-FREE $MASnI_3$ PEROVSKITE-BASED SOLAR CELL USING INORGANIC CHARGE TRANSPORT LAYERS

Matthew I. Amanyi[a], Abubakar S. Yusuf[b], Eghwubare Akpoguma[c], Stephen O. Eghaghe[d], James Eneye[d], Raymond M. Agaku[e], Lilian C. Echebiri[f], Emmanuel U. Echebiri[g], Emmanuel O. Ameh[f], Chinyere I. Eririogu[h], Nicholas N. Tasie[i], Anthony C. Ozurumba[j], Eli Danladi[a,*]

[a]*Department of Physics, Federal University of Health Sciences, Otukpo, Benue State, Nigeria*
[b]*Department of Physics, Federal University of Technology, Minna, Niger State, Nigeria*
[c]*Nuclear Technology Center, Nigeria Atomic Energy Commision, Abuja, Nigeria*
[d]*Department of Physics, Bingham University, Nasarawa State, Nigeria*
[e]*Department of Physics, Benue State University, Benue State, Nigeria*
[f]*Department of Physics, Nasarawa State University, Nasarawa State, Nigeria*
[g]*Department of Electrical/Electronic Engineering, Nile University of Nigeria*
[h]*Department of Physics, University of Nigeria Nnsukka, Enugu State, Nigeria*
[i]*Department of Physics, Rivers State University, Port Harcourt, Rivers State, Nigeria*
[j]*Africa Center of Excellence in Future Energies and Electrochemical Systems, Federal Univerity of Technology, Owerri, Imo State, Nigeria*
**Corresponding Author e-mail: danladielibako@gmail.com*
Received May 31, 2024; revised July 17, 2024; in final form August 19, 2024; accepted August 19, 2024

Perovskite solar cells (PSCs) have gained a lot of attention due to their high efficiency and low cost. In this research paper, a methylammonium tin iodide ($CH_3NH_3SnI_3$) based solar cell was simulated using a one-dimensional solar cell capacitance simulation (SCAPS-1D) tool. The SCAPS-1D tool is based on Poisson and the semiconductor equations. After thorough investigation, the initial device presents the following parameters; power conversion efficiency (PCE)=15.315%, fill factor (FF)=64.580%, current density (J_{sc})=29.152 mA/cm^{2,} and open circuit voltage (V_{oc})=0.813 V. The effect of absorber and ETL thicknesses were explored systematically. The performance of the simulated device was significantly influenced by the thickness of the absorber and ETL. The optimized absorber thickness was 0.5 µm and the ETL thickness was 0.02 µm, giving rise to an optimized PCE of 15.411%, FF of 63.525%, J_{sc} of 29.812 mA/cm^2, and V_{oc} of 0.814 V. Additionally, the effect of temperature on the optimized device was evaluated and found that it affects the performance of the device. This model shows the prospect of $CH_3NH_3SnI_3$ as a perovskite material to produce toxic-free environment-friendly solar cells with high efficiency.
Keywords: *Perovskite solar cell; SCAPS-1D; $CH_3NH_3SnI_3$; Photovoltaic*
PACS: 41.20.Cv; 61.43.Bn; *68.55.ag*; *68.55.jd*; 73.25.+i; 72.80.Tm

INTRODUCTION

To maintain the current state of growth in the photovoltaic domain, perovskite solar cells have received significant attention due to the fast pace of efficiency growth from 3.8 to >25% in just over a decade of research [1], [2], [3], [4]. The enhancement in efficiency is attributed to the excellent optoelectronic characteristics of the absorbing halide perovskite materials, amongst which include; long-range charge diffusion lengths, high absorption coefficient, low exciton binding energies, tunable band gaps, and high charge carrier mobilities [5], [6], [7], [8], [9]. As light absorbers in PSCs, hybrid organic−inorganic halide absorbing materials which include the methylammonium lead triiodide ($MAPbI_3$) and formamidinium lead triiodide ($FAPbI_3$) has been at the forefront of research in the photovoltaic horizon. One of the challenges that limited its commercialization and effective utilization is the presence of lead (Pb), which is toxic in nature [6], [10], [11]. Under these situations, the European Union and other nations have placed great restrictions on the use of Pb-containing materials in electronic devices, which has triggered interest in Pb-free PSCs [12], [13].

In overcoming the challenge of high toxicity, researchers have devoted enormous efforts to replacing lead with eco-friendly materials such as tin (Sn), Bismuth (Bi), and Germanium (Ge) [14]. Amongst the listed eco-friendly perovskite crystals, Sn-based perovskite is receiving the greatest attention.

Due to the low toxicity and exceptional theoretical PCE, tin halide-based perovskites have gained a lot of attention in the development of PSCs [15]. Sn is considered one of the most practical substitutes for Pb in the perovskite configurations as a replacement of the toxic Pb^{2+} ions with Sn^{2+} creating no distortion in the perovskite structure owing to the similarity between the outer shell of Pb and Sn [15], [16]. In this category are the methylammonium tin triiodide ($MASnI_3$), cesium tin triiodide ($CsSnI_3$), and formamidine tin iodide ($FASnI_3$). However, the $MASnI_3$ perovskite is achieving good efficiency and is the closest candidate among the other Pb-free based absorbers due to (i) its direct bandgap of 1.30 eV which has an ideal bandgap close to those postulated by the Shockley-Queisser limit [17] and (ii) highest light absorption properties and high optical behavior to be used in optoelectronic devices [18], hence it was utilized in our present study.

Cite as: M.I. Amanyi, A.S. Yusuf, E. Akpoguma, S.O. Eghaghe, J. Eneye, R.M. Agaku, L.C. Echebiri, E.U. Echebiri, E.O Ameh, C.I. Eririogu, N.N. Tasie, A.C. Ozurumba, E. Danladi, East Eur. J. Phys. 3, 447 (2024), https://doi.org/10.26565/2312-4334-2024-3-54

The conventional PSC configuration is made up of two charge transport layers, an electron transport layer (ETL), a hole transport layer (HTL), and a perovskite absorption layer. The ETL plays a crucial role by conveying photogenerated electrons and blocking holes. Some examples of commonly used ETL are TiO_2, SnO_2, Nb_2O_5, Al_2O_3, PCBM, C60, WOx, ZnO, I_2O_3, $BaTiO_3$, and $PbTiO_3$ [19], [20]. The HTL plays a crucial role by conveying photogenerated holes and blocking electrons. Polymeric HTLs and inorganic or organic small molecules can be categorized into several groups depending on their chemical composition, according to established categorization methods [21]. Among these types of HTLs, $CuSbS_2$, NiO, P3HT, Cu_2O, CuSCN, PEDOT: PSS, CuI, CuO, NiO, and SpiroMeOTAD are commonly used in several studies [19], [20], [21]. Due to the wide band gap, better energy level, and environmental stability, TiO_2 is one of the highly utilized ETLs [22]. Also, the suitable band gap, good stability, and desirable band bending make TiO_2 one of the best ETLs to be used with the $MASnI_3$ perovskite absorber material, hence it was utilized in our study.

In this study, an eco-friendly PSC based on $MASnI_3$ was modeled and simulated using SCAPS-1D software with TiO_2 as an efficient electron transport layer. We thoroughly explored the effect of different layer parameters including ETL thickness and absorber thickness to obtain an optimized PSC device. We subsequently investigated the thermal effect on the optimized device. These parameters help to identify the best solar cell characteristics and significantly increase power conversion efficiency. These findings now open up a fruitful research opportunity for developing and manufacturing low-cost, highly efficient, lead-free perovskite solar cells.

2. METHODOLOGY AND SIMULATION

In this study, the Solar Cell Capacitance Simulator (SCAPS-1D) software was utilized to carry out the investigation [23]. Several simulation software have been used in the study of PSC. Amongst these include; SILVACO ATLAS, AMPS, COMSOL, and SCAPS [16], [24], [25], [26]. The SCAPS-1D is advantaged over other tools listed above, which include its ability to simulate up to seven different layers without routine measurements. It can allow the calculations of many parameters such as spectral response, energy bands, ac characteristics, *J*−*V* curve, Q-E curve, and defect density, by simply resolving the basic equations of semiconductor [22].

Equation 1 [22] illustrates the relationship between charges to electrostatic potential.

$$\frac{d^2}{dx^2}\psi(x) = \frac{q}{\varepsilon_0\varepsilon_r}[p(x) - n(x) + N_D - N_A + \rho_P - \rho_n], \tag{1}$$

where ψ is the electrostatic potential, $n(x)$ and $p(x)$ are densities of electrons and holes, ε_r is the relative permittivity, ε_0 is the permittivity of free space, the donor and accepted impurities are denoted as N_D and N_A, ρ_P and ρ_n, are the distributions of holes and electrons, q is the charge.

Equations (2) and (3) show how the density gradients, current densities, and net generation of electrons and holes are conserved [27].

$$\frac{\partial n}{\partial t} = \frac{1}{q}\frac{\partial J_n}{\partial x} + (G_n - R_n), \tag{2}$$

$$\frac{\partial p}{\partial t} = \frac{1}{q}\frac{\partial J_p}{\partial x} + \left(G_p - R_p\right), \tag{3}$$

where G is the generation, R is the recombination, J_n is the electron density, J_p is the density of holes.

The total currents, J_n and J_p resulted by the drift and diffusion of charge carriers which can be used to obtain the current densities of the solar cells.

In the present study, the HTL is considered as the p-type layer, the ETL as the n-type of the $MASnI_3$-based perovskite, the transparent oxide here is represented as fluorine-doped tin oxide (FTO), and gold (Au) as the back metal contact (BMC) for the device.

To have a successful simulation in this work, the layer's parameters were chosen carefully from experimental results and other theoretical research in the literature. The details for each layer are summarized in Table 1 [15], [16], [22].

Table 1. Parameters used for simulation of perovskite solar cell structures using SCAPS-1D

Parameters	FTO	ETL	Absorber	HTL
Thickness (μm)	0.4	0.05	0.40	0.15
E_g (eV)	3.5	3.2	1.30	2.17
χ (eV)	4.0	4.2	4.20	3.2
ϵ_r	9	10.0	8.2	7.11
N_C (cm^{-3})	2.2×10^{18}	2.2×10^{18}	1.0×10^{18}	2.2×10^{18}
N_V (cm^{-3})	1.8×10^{19}	2.2×10^{18}	1.0×10^{18}	2.2×10^{18}
μ_n ($cm^2\ V^{-1}\ s^{-1}$)	20	20	1.6	80
μ_p ($cm^2\ V^{-1}\ s^{-1}$)	10	10	1.6	80
N_D (cm^{-3})	1×10^{18}	1×10^{17}	0	0
N_A (cm^{-3})	0	0	3.2×10^{15}	1.0×10^{18}
N_t (cm^{-3})	1×10^{15}	1×10^{15}	4.5×10^{16}	1.0×10^{15}

Additionally, Table 2 provides the interface defect properties of the input parameters. The work function (W_F) of front and back contacts are 4.40 eV and 5.10 eV. The scanning voltage is taken from 0-1.6 V, and the temperature during the simulation was set at 300 K. The simulation evaluation is completed under 100 mW/cm^2 light intensity. The thermal velocities of the hole and electron is 10^7 cms^{-1}**.** During the optimization process, the parameters of FTO, $MASnI_3$, and HTL are kept constant and the thickness of ETL is varied from 0.01 to 0.1 µm to get the optimum performance parameters. Also, for $MASnI_3$, the parameters of FTO, ETL, and HTL were kept constant while varying $MASnI_3$ thickness from 0.1 to 1.0 µm to get the optimum performance parameter. For the optimized temperature, the parameters of the optimized device were kept constant while the temperature was varied from 290 to 360 K to get the optimum metric parameters. The simulated device and energy profile are shown in Figure 1.

Table 2. Parameters of interface layer

Parameters	**TiO_2/$CH_3NH_3SnI_3$ interface**	**$CH_3NH_3SnI_3$/Cu_2O interface**
Defect type	Neutral	Neutral
Capture cross section for electrons (cm^2)	1×10^{-15}	1×10^{-15}
Capture cross section for holes (cm^2)	1×10^{-15}	1×10^{-15}
Energetic distribution	Single	Single
Energy level with respect to Ev (eV)	0.600	0.600
Characteristic energy (eV)	0.1	0.1
Total density (cm^{-3})	1×10^{10}	1×10^{-10}

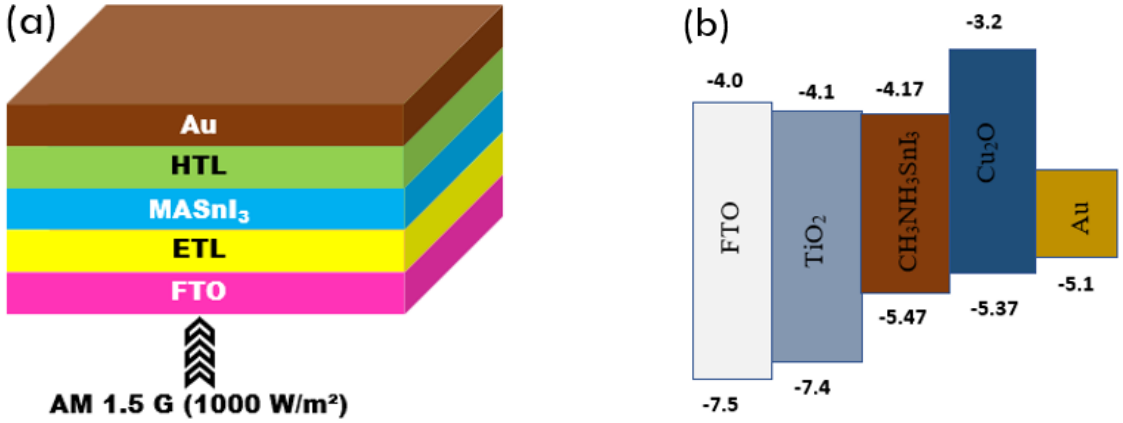

Figure 1. (a) Device Structure and (b) Energy Band Profile

3. RESULTS AND DISCUSSION

3.1. Analysis of initial device

With the parameters available in Tables 1 and 2, the results of current-voltage, quantum efficiency, and power density were obtained as shown in Figure 2a-c.

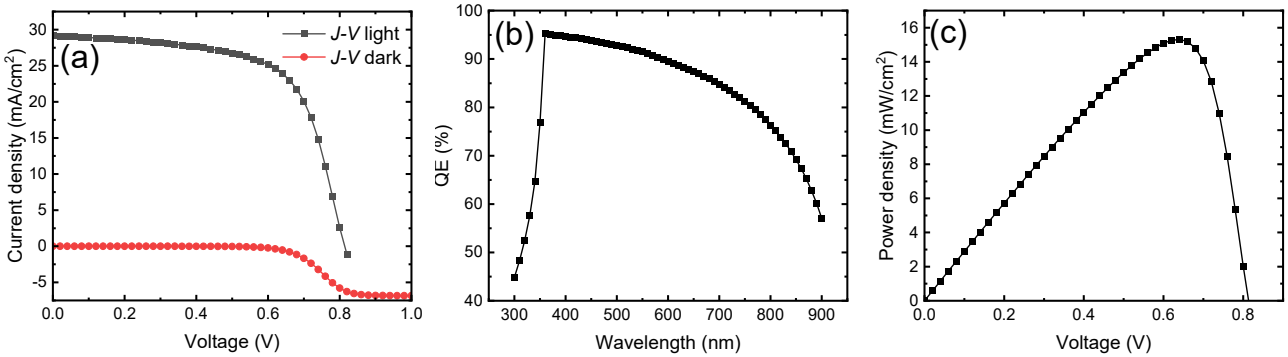

Figure 2. (a) *J–V* curve of PSC in the light and dark conditions, (b) QE with respect to wavelength, and (c) *P-V* curve

Table 3 shows the photovoltaic characteristics of the $MASnI_3$ cell, which include; open circuit voltage (V_{oc}), short circuit current (J_{sc}), fill factor (FF), and power conversion efficiency (PCE). To verify our theoretical assertion, the results were compared with other findings [15], [28], [29]. Our results show a PCE of 15.315%, FF of 64.580%, V_{oc} of 0.813 V, and a J_{sc} of 29.152 mA/cm^2. The agreement with other studies shows that the device simulation is valid

and the input parameters are close to established real devices. In the dark condition, the device acts as a diode as depicted in Figure 2a. The depletion layer spreads, the internal electric field expands, and the electrons' electric potential energy rises when a bias voltage is given to the Schottky barrier [22]. Figure 2b shows the QE vs. wavelength. As can be seen, the QE rises with an increase in wavelength from 45% at 300 nm to 95% at 350 nm. The QE covers the entire visible spectrum and reaches a broad absorption maximum before it starts declining to 900 nm. This agrees with similar studies [15], [16], [30]. The sweeping at the visible and near-infrared region is significantly beneficial to the absorption of light at various wavelengths. The power density is shown in Figure 2c with a maximum power density of 15.315 mW/cm^2.

Table 3. Electrical parameters with varied absorber thickness

Thickness (µm)	PCE (%)	*FF* (%)	J_{sc} (mA/cm^2)	V_{oc} (V)
0.1	10.774	74.706	17.353	0.831
0.2	14.064	70.615	24.348	0.818
0.3	15.090	67.032	27.656	0.814
0.4	15.315	64.580	29.152	0.813
0.5	15.321	63.284	29.763	0.813
0.6	15.306	62.849	29.942	0.813
0.7	15.296	62.760	29.965	0.813
0.8	15.288	62.730	29.963	0.813
0.9	15.280	62.702	29.961	0.813
1.0	15.272	62.673	29.960	0.813

3.2. Optimization of absorber layer thickness

The absorbing material in perovskite solar cells is significantly responsible for all photovoltaic processes, which include the generation, recombination, and transportation of charge carriers, hence often called the heart of the solar cell. Numerous studies have shown that the quality of the perovskite layer greatly influences the lifetime and diffusion length of photo-generated carriers, which in turn affect the overall performance of the solar cell [31], [32]. To improve the solar cell performance, the optimization of the absorber layer is highly indispensable. If the absorber layer thickness is greater than the diffusion length, then the generated charge carriers will recombine at the layer, and the series resistance of the solar cell will increase as a result, the charge carriers cannot reach the electrode [32]. When the thickness is too thin, a low absorption rate is observed which results in reduced photocurrent value. Therefore, getting the optimized thickness of the absorber layer is crucial for high-performing PSCs [33]. In this study, absorber thickness was varied from 0.1 to 1.0 µm, at an interval of 0.1 µm to obtain the optimized value. The results are presented in Figures 3 and 4. Fig. 3a shows the *J-V* curve at different thicknesses and Fig. 3b presents the QE at different thicknesses. From the result, the PCE increases with increasing absorber layer thickness until the thickness achieves a value of 0.5 µm. The initial increase in PCE is attributed to increase in electron-hole pair generation rate inside the absorber layer [32].

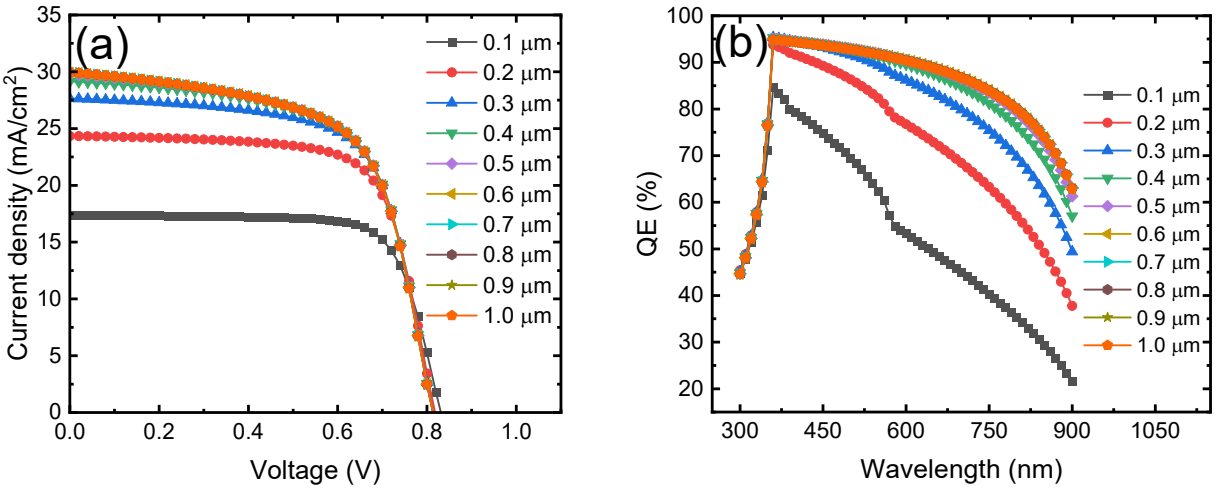

Figure 3. (a) *J–V* curve of PSC with different absorber thickness and (b) QE with respect to wavelength of different absorber thickness

When the thickness goes beyond 0.5 µm, the PCE values decline which makes the choice of the optimal thickness to be 0.5 µm which corresponds to the photovoltaic properties of PCE=15.321%, FF=63.284%, J_{sc}=29.763 mA/cm^2, and V_{oc}=0.813 V. The decrease in PCE when the thickness exceeds 0.5 µm is attributed to increase in recombination rate of charge carrier [15]. It can be seen that the V_{oc} decreases when the thickness of the absorbing layers increases from 0.1 to 0.3 µm, thereafter, it maintains a constant value which is the point of saturation. The FF decreases with an increase in the

absorber thickness (see Table 3). The decrease in FF is attributed to the increase in series resistance [32]. The relationship between absorber layer thickness with the photovoltaic parameters (PCE, FF, J_{sc}, and V_{oc}) is depicted in Figure 4a-d.

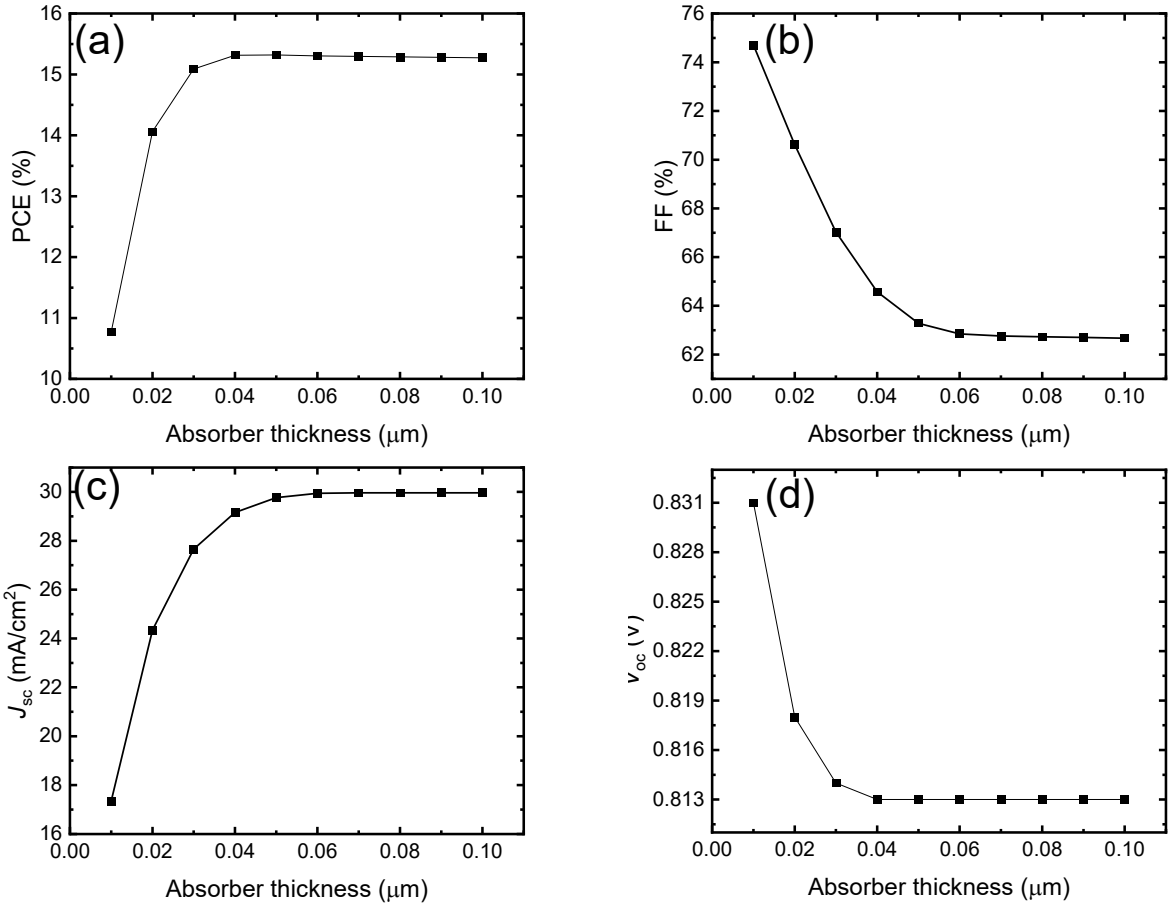

Figure 4. (a) variation of PCE with absorber thickness, (b) variation of FF with absorber thickness, (c) variation of J_{sc} with absorber thickness, and (d) variation of V_{oc} with absorber thickness

3.3. Optimization of ETL layer thickness

The performance of PSC is highly impacted by the thickness of the ETL. Crucially, the choice of proper ETL plays a great role in the design and implementation of high-performing PSC as the band alignment between the absorber and ETL layer is an important factor for improved PSCs [15], [34]. Fig. 5a shows the *J-V* curve with varied ETL thickness while Fig. 5b shows the QE characteristics with varied ETL thickness.

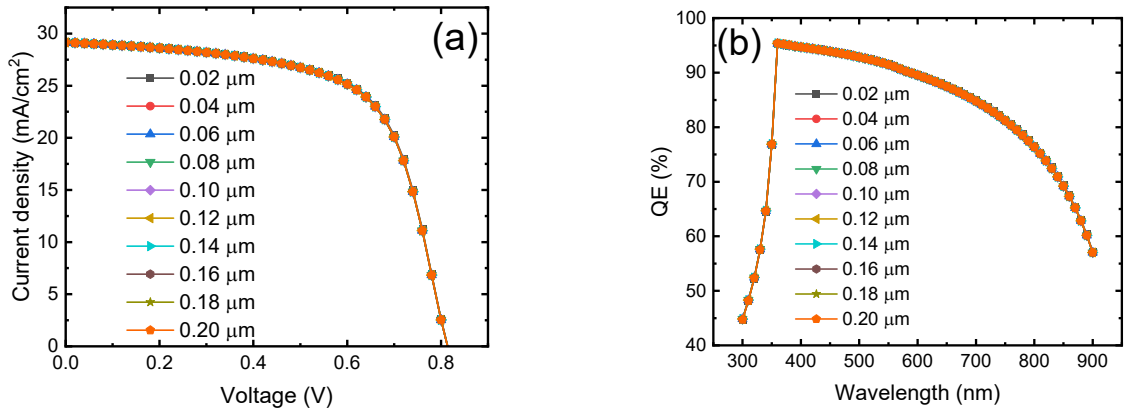

Figure 5. (continued on the next page). (a) *J–V* curve of PSC with different ETL thickness, (b) QE with respect to wavelength with different ETL thickness, (c) variation of PCE and FF with ETL thickness, and (d) variation of J_{sc} and V_{oc} with absorber thickness

The variation of performance parameters which include the PCE, FF, $J_{sc,}$ and V_{oc} with thicknesses of the ETL is shown in Figures 5c & d. As shown in Table 5, the PCE decreases gently from 15.399 to 15.302% as the thickness rose from 0.02 to 0.20 μm. The increase in ETL thickness decreases the J_{sc} of the PSCs by correspondingly increasing photon

absorption and resistance of the cell (see Figure 5b). The increase in QE with increasing photon energies can be seen to arise from the absorption coefficient within the regions and the consequence of increased density of localized states in the gap itself due to the rise in new defect states [35]. The increase in ETL thickness results in partial absorption of light, which slows down the pace of charge formation and collection and prevents enough light from reaching the absorber as a result leading to a decrease in transmittance and reduced performance [5]. The optimized ETL thickness was found to be 0.02 µm which gave PCE, FF, $J_{sc,}$ and V_{oc} values of 15.399%, 64.830%, 29.186 mA/cm^{2,} and 0.814 V.

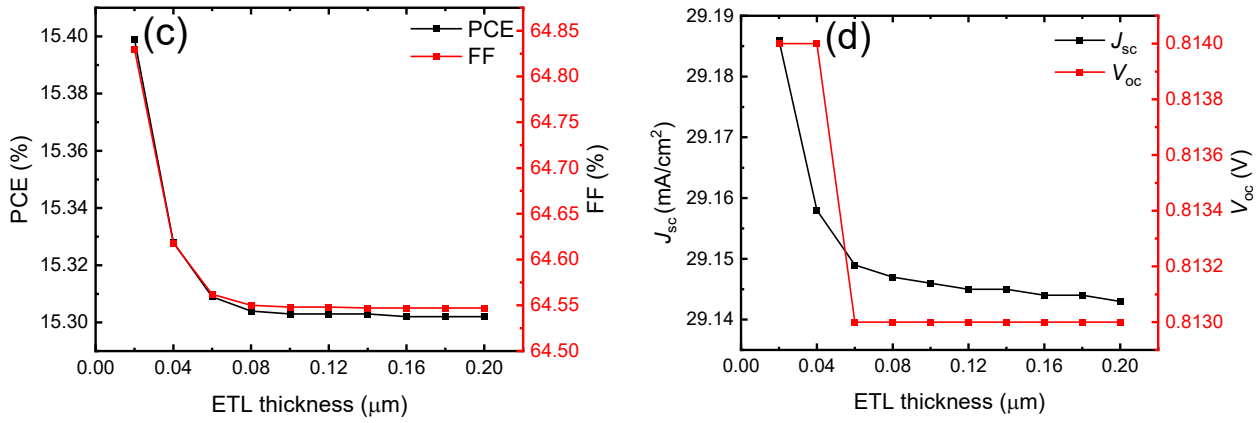

Figure 5. (continuation). (a) *J–V* curve of PSC with different ETL thickness, (b) QE with respect to wavelength with different ETL thickness, (c) variation of PCE and FF with ETL thickness, and (d) variation of J_{sc} and V_{oc} with absorber thickness

Table 5. Electrical parameters with varied ETL thickness

Thickness (µm)	PCE (%)	*FF* (%)	J_{sc} (mA/cm^2)	V_{oc} (V)
0.02	15.399	64.830	29.186	0.814
0.04	15.328	64.618	29.158	0.814
0.06	15.309	64.562	29.149	0.813
0.08	15.304	64.550	29.147	0.813
0.10	15.303	64.548	29.146	0.813
0.12	15.303	64.548	29.145	0.813
0.14	15.303	64.547	29.145	0.813
0.16	15.302	64.547	29.144	0.813
0.18	15.302	64.547	29.144	0.813
0.20	15.302	64.547	29.143	0.813

3.4. Optimized simulated PSC

Following the PSC simulation, the thickness of the absorber and the thickness of the ETL were optimized. The results show that the optimized absorber thickness is 0.5 µm and the ETL thickness is 0.02 µm. The *J-V* and QE curves for the optimized and unoptimized devices are shown in Figure 6a & b.

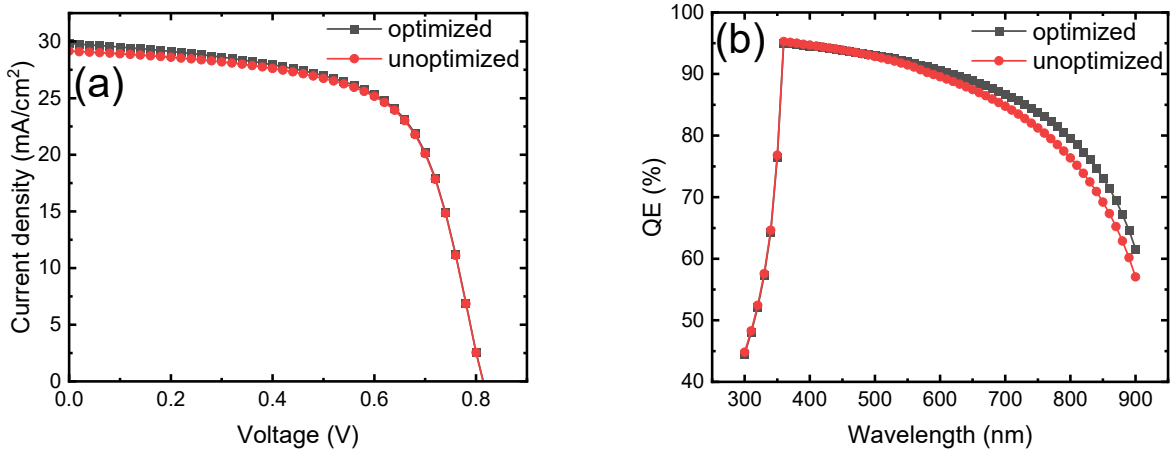

Figure 6. (a) *J–V* of the optimized (black) and unoptimized (red) and (b) QE curves of the optimized (black) and unoptimized (red)

The final optimized PSC gave a turnover PCE of 15.411%, FF of 63.525%, J_{sc} of 29.812 mA/cm^2, and V_{oc} of 0.814 V. By enhancing the film quality of the absorber and ETL, a satisfactory electron density can be attained. The quantum efficiency also shows stronger absorption in the visible region and near IR region for the optimized device.

3.5. Effect of Temperature on the optimized PSC device

Temperature is one of the crucial factors that influence the performance of solar cells. It is very important to carefully look at the optimal solar cell's performance in relation to operating temperature. Figure 7a shows the *J-V* curve with temperature variation (from 280-360 K), while Figure 7b & c illustrate the PCE & FF and J_{sc} & V_{oc} with temperature dependence. When the temperature was raised from 280 to 360 K, the PCE, $J_{sc,}$ and V_{oc} declined steadily. Practically, a rise in temperature leads to the recombination of carriers, but it also causes a significant increase in FF partly due to higher phonon motions and collisions (see Table 6).

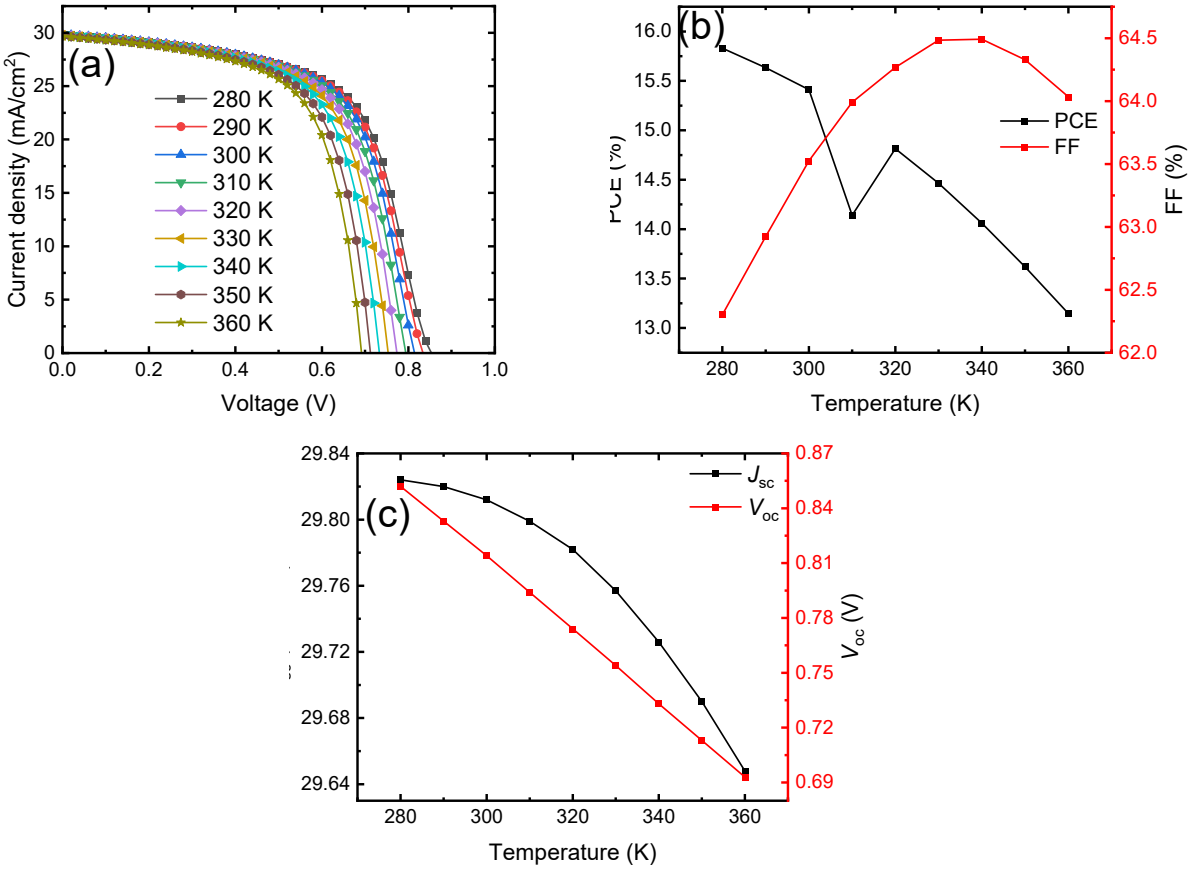

Figure 7. (a) *J-V* with varied temperature under illumination, (b) PCE and FF with respect to varied temperature, and (c) J_{sc} and V_{oc} with respect to varied temperature

Table 6. Electrical parameters based on varied Temperature

Temperature (K)	PCE (%)	*FF* (%)	J_{sc} (mA/cm^2)	V_{oc} (V)
280	15.830	62.301	29.824	0.852
290	15.633	62.923	29.820	0.833
300	15.411	63.525	29.812	0.814
310	14.140	63.990	29.799	0.794
320	14.814	64.267	29.782	0.774
330	14.464	64.484	29.757	0.754
340	14.061	64.491	29.726	0.733
350	13.619	64.329	29.690	0.713
360	13.147	64.034	29.648	0.693

The FF experienced a decrease after 350 K. The drop in FF may be attributed to lower stability, higher recombination rate, and longer lifetimes associated with carriers in the absorber [22]. The V_{oc} decrease is attributed to lattice expansion and interatomic bond attenuation brought on by higher temperatures [36]. Also, the rise in saturation current is the reason for the decrease in PCE, which also results in an increase in recombination rate [37]. At greater temperatures, defects or trap states, for example, may become active non-radiative recombination centers [22]. These centers provide carriers with an additional path for recombination without emitting photons, which increases the overall recombination rate and may lessen the contribution from radiative recombination.

4. CONCLUSIONS

In this research, the one-dimensional solar cell capacitance simulator (SCAPS-1D) software was utilized to perform a numerical simulation on a lead-free $MASnI_3$-based perovskite solar cell. The device structure is composed of TiO_2 as

ETL, $MASnI_3$ as absorbing material, and Cu_2O as HTL in a configuration FTO/TiO_2/$MASnI_3$/Cu_2O/Au. The simulation of the initial device gave a turnover output of 15.315%, 64.580%, 29.152 mA/cm^{2,} and 0.813 V for PCE, FF, J_{sc}, and V_{oc}. The effect of absorber and ETL thicknesses were explored to obtain optimized values of 0.5 and 0.02 µm, resulting in PCE of 15.411%, FF of 63.525%, J_{sc} of 29.812 mA/cm^2, and V_{oc} of 0.814 V. The effect of temperature was studied by varying the temperature from 280-360 K. The device's efficiency decreases with increasing temperature which can be attributed to the rise in saturation current leading to an increase in recombination rate. The results obtained are somewhat encouraging and have paved the path for developing cost-effective, eco-friendly, and comparable state-of-the-art, high-efficiency perovskite solar cells.

Acknowledgments

The authors would like to thank Professor Marc Burgelman and his team at the Department of Electronics and Information Systems, University of Gent for the development of the SCAPS software package and for allowing its use.

ORCID

Abubakar S. Yusuf, https://orcid.org/0000-0001-8181-9728; **Nicholas Tasie**, https://orcid.org/0000-0001-8398-2596
Anthony C. Ozurumba, https://orcid.org/0009-0003-2269-7742; **Eli Danladi,** https://orcid.org/0000-0001-5109-4690

REFERENCES

[1] A. Kojima, K. Teshima, Y. Shirai, and T. Miyasaka, "Organometal Halide Perovskites as Visible-Light Sensitizers for Photovoltaic Cells," J. Am. Chem. Soc. **131**(17), 6050–6051 (2009). https://doi.org/10.1021/ja809598r
[2] E. Danladi, *et al*., "Defect and doping concentration study with series and shunt resistance influence on graphene modified perovskite solar cell: A numerical investigation in SCAPS-1D framework," Journal of the Indian Chemical Society, **100**(5), 101001 (2023). https://doi.org/10.1016/j.jics.2023.101001
[3] E. Danladi *et al*., "Broad-band-enhanced and minimal hysteresis perovskite solar cells with interfacial coating of biogenic plasmonic light trapping silver nanoparticles," Materials Research Innovations, **27**(7), 521–536 (2023). https://doi.org/10.1080/14328917.2023.2204585
[4] Z. Qu, F. Ma, Y. Zhao, X. Chu, S. Yu, and J. You, "Updated Progresses in Perovskite Solar Cells," Chinese Phys. Lett. **38**(10), 107801 (2021). https://doi.org/10.1088/0256-307X/38/10/107801
[5] M.K. Hossain, *et al*., "Numerical simulation and optimization of a $CsPbI_3$-based perovskite solar cell to enhance the power conversion efficiency," New J. Chem. **47**(10), 4801–4817 (2023). https://doi.org/10.1039/D2NJ06206B
[6] M.K. Hossain, *et al*., "Deep Insights into the Coupled Optoelectronic and Photovoltaic Analysis of Lead-Free $CsSnI_3$ Perovskite-Based Solar Cell Using DFT Calculations and SCAPS-1D Simulations," ACS Omega, **8**(25), 22466–22485 (2023). https://doi.org/10.1021/acsomega.3c00306
[7] S.D. Stranks, and H. J. Snaith, "Metal-halide perovskites for photovoltaic and light-emitting devices," Nature Nanotech. **10**(5), 391–402 (2015). https://doi.org/10.1038/nnano.2015.90
[8] Md.R. Islam, A.A.M. Mazumder, Md.R.H. Mojumder, A.S.M.Z. Shifat, and M.K. Hossain, "Strain-induced tunable optoelectronic properties of inorganic halide perovskites $APbCl_3$ (A = K, Rb, and Cs)," Jpn. J. Appl. Phys. **62**(1), 011002 (2023). https://doi.org/10.35848/1347-4065/acb09e
[9] A. Thakur, D. Singh, and S.K. Gill, "Numerical simulations of 26.11% efficient planar $CH_3NH_3PbI_3$ perovskite n-i-p solar cell," Materials Today: Proceedings, **71**, 195–201 (2022). https://doi.org/10.1016/j.matpr.2022.08.423
[10] H. Bencherif, *et al*., "Performance enhancement of $(FAPbI3)_{1-x}(MAPbBr_3)_x$ perovskite solar cell with an optimized design," Micro and Nanostructures, **171**, 207403 (2022). https://doi.org/10.1016/j.micrna.2022.207403
[11] H. Bencherif, and M.K. Hossain, "Design and numerical investigation of efficient $(FAPbI_3)_{1-x}(CsSnI_3)_x$ perovskite solar cell with optimized performances," Solar Energy, **248**, 137–148 (2022). https://doi.org/10.1016/j.solener.2022.11.012
[12] Y. Zhou, and K. Zhu, "Perovskite Solar Cells Shine in the 'Valley of the Sun,'" ACS Energy Lett. **1**(1), 64–67 (2016). https://doi.org/10.1021/acsenergylett.6b00069
[13] B.V. Lotsch, "New Light on an Old Story: Perovskites Go Solar," Angew Chem. Int. Ed. **53**(3), 635–637 (2014). https://doi.org/10.1002/anie.201309368
[14] H. Sabbah, "Numerical Simulation of 30% Efficient Lead-Free Perovskite $CsSnGeI_3$-Based Solar Cells," Materials, **15**(9), 3229 (2022). https://doi.org/10.3390/ma15093229
[15] E. Danladi, A.O. Salawu, M.O. Abdulmalik, E.D. Onoja, E.E. Onwoke, and D.S. Adepehin, "Optimization of Absorber and ETM Layer Thickness for Enhanced Tin based Perovskite Solar Cell Performance using SCAPS-1D Software," PA, **02**(01), 1–11 (2022). https://doi.org/10.47514/phyaccess.2022.2.1.001
[16] E. Danladi, M. Kashif, A. Ichoja, and B. B. Ayiya, "Modeling of a Sn-Based HTM-Free Perovskite Solar Cell Using a One-Dimensional Solar Cell Capacitance Simulator Tool," Trans. Tianjin Univ. **29**(1), 62–72 (2023). https://doi.org/10.1007/s12209-022-00343-w
[17] W. Shockley, and H.J. Queisser, "Detailed Balance Limit of Efficiency of p-n Junction Solar Cells," Journal of Applied Physics, **32**(3), 510–519 (1961). https://doi.org/10.1063/1.1736034
[18] D. Jalalian, A. Ghadimi, and A. Kiani, "Modeling of a high performance bandgap graded Pb-free HTM-free perovskite solar cell," Eur. Phys. J. Appl. Phys. **87**(1), 10101 (2019). https://doi.org/10.1051/epjap/2019190095
[19] M.K. Hossain, *et al*., "An extensive study on multiple ETL and HTL layers to design and simulation of high-performance lead-free $CsSnCl_3$-based perovskite solar cells," Sci. Rep. **13**(1), 2521 (2023). https://doi.org/10.1038/s41598-023-28506-2
[20] M.K. Hossain, *et al*., "Numerical Analysis in DFT and SCAPS-1D on the Influence of Different Charge Transport Layers of $CsPbBr_3$ Perovskite Solar Cells," Energy Fuels, **37**(8), 6078–6098 (2023). https://doi.org/10.1021/acs.energyfuels.3c00035
[21] J. Chen, and N.-G. Park, "Inorganic Hole Transporting Materials for Stable and High Efficiency Perovskite Solar Cells," J. Phys. Chem. C, **122**(25), 14039–14063 (2018). https://doi.org/10.1021/acs.jpcc.8b01177
[22] E. Danladi, *et al*., "Highly efficient, hole transport layer (HTL)-free perovskite solar cell based on lithium-doped electron transport layer by device simulation," Emergent Mater. **6**(6), 1779–1795 (2023). https://doi.org/10.1007/s42247-023-00558-0

[23] M.K.A. Mohammed, "High-performance hole conductor-free perovskite solar cell using a carbon nanotube counter electrode," RSC Adv. **10**(59), 35831–35839 (2020). https://doi.org/10.1039/D0RA05975G
[24] N. Fakhri, M.S. Naderi, S.G. Farkoush, S.S. Nahaei, S.-N. Park, and S.-B. Rhee, "Simulation of Perovskite Solar Cells Optimized by the Inverse Planar Method in SILVACO: 3D Electrical and Optical Models," Energies, **14**(18), 5944 (2021). https://doi.org/10.3390/en14185944
[25] S. Zandi, P. Saxena, and N.E. Gorji, "Numerical simulation of heat distribution in RGO-contacted perovskite solar cells using COMSOL," Solar Energy, **197**, 105–110 (2020). https://doi.org/10.1016/j.solener.2019.12.050
[26] M.K. Hossain, M.H.K. Rubel, G.F.I. Toki, I. Alam, Md.F. Rahman, and H. Bencherif, "Effect of Various Electron and Hole Transport Layers on the Performance of CsPbI 3 -Based Perovskite Solar Cells: A Numerical Investigation in DFT, SCAPS-1D, and wxAMPS Frameworks," ACS Omega, **7**(47), 43210–43230 (2022). https://doi.org/10.1021/acsomega.2c05912
[27] E. Danladi, *et al*., "Modeling and simulation of > 19% highly efficient PbS colloidal quantum dot solar cell: A step towards unleashing the prospect of quantum dot absorber," Optik, **291**, 171325 (2023). https://doi.org/10.1016/j.ijleo.2023.171325
[28] P.K. Jha, *et al*., "Study of Eco-Friendly Organic–Inorganic Heterostructure $CH_3NH_3SnI_3$ Perovskite Solar Cell via SCAPS Simulation," J. Electron. Mater. **52**(7), 4321–4329 (2023). https://doi.org/10.1007/s11664-023-10267-3
[29] K. Nishimura, *et al*., "Lead-free tin-halide perovskite solar cells with 13% efficiency," Nano Energy, **74**, 104858 (2020). https://doi.org/10.1016/j.nanoen.2020.104858
[30] H.-J. Du, W.-C. Wang, and J.-Z. Zhu, "Device simulation of lead-free $CH_3NH_3SnI_3$ perovskite solar cells with high efficiency," Chinese Phys. B, **25**(10), 108802 (2016). https://doi.org/10.1088/1674-1056/25/10/108802
[31] Guo, *et al*., "Effects of Transition Metal Substituents on Interfacial and Electronic Structure of $CH_3NH_3PbI_3/TiO_2$ Interface: A First-Principles Comparative Study," Nanomaterials, **9**(7), 966 (2019). https://doi.org/10.3390/nano9070966
[32] N.J. Valeti, K. Prakash, and M.K. Singha, "Numerical simulation and optimization of lead free $CH_3NH_3SnI_3$ perovskite solar cell with $CuSbS_2$ as HTL using SCAPS 1D," Results in Optics, **12**, 100440 (2023). https://doi.org/10.1016/j.rio.2023.100440
[33] M. Liu, M.B. Johnston, and H.J. Snaith, "Efficient planar heterojunction perovskite solar cells by vapour deposition," Nature, **501**(7467), 395–398 (2013). https://doi.org/10.1038/nature12509
[34] O.A. Muhammed, E. Danladi, P.H. Boduku, J. Tasiu, M.S. Ahmad, and N. Usman, "Modeling and Simulation of Lead-Free Perovskite Solar Cell Using SCAPS-1D," EEJP, (2), 146-154 (2021). https://doi.org/10.26565/2312-4334-2021-2-12
[35] N.F. Mott, and E.A. Davis, *Electronic processes in non-crystalline materials, 2nd ed. in International series of monographs on physics*, (Clarendon Press, Oxford, 2012).
[36] I. Qasim, *et al*., "Numerical optimization of (FTO/ZnO/CdS/$CH_3NH_3SnI_3$/GaAs/Au) perovskite solar cell using solar capacitance simulator with efficiency above 23% predicted," Opt. Quant. Electron. **53**(12), 713 (2021). https://doi.org/10.1007/s11082-021-03361-5
[37] S. Ahmed, F. Jannat, Md.A.K. Khan, and M.A. Alim, "Numerical development of eco-friendly Cs_2TiBr_6 based perovskite solar cell with all-inorganic charge transport materials via SCAPS-1D," Optik, **225**, 165765 (2021). https://doi.org/10.1016/j.ijleo.2020.165765

SCAPS-1D АНАЛІЗ НЕТОКСИЧНИХ БЕЗСВИНЦЕВИХ СОНЯЧНИХ ЕЛЕМЕНТІВ НА ОСНОВІ ПЕРОВСКІТУ $MASnI_3$ З ВИКОРИСТАННЯМ НЕОРГАНІЧНИХ ШАРІВ ТРАНСПОРТУ ЗАРЯДУ

Меттью І. Амані[a], Абубакар С. Юсуф[b], Егвубаре Акпогума[c], Стівен О. Егаге[d], Джеймс Енейе[d], Раймонд М. Агаку[e], Ліліан С. Ечебірі[f], Еммануель У. Ечебірі[g], Еммануель О. Аме[f], Чіньєре І. Ерірогу[h], Ніколас Н. Тасі[i], Ентоні С. Озурумба[j], Елі Данладі[a]

[a]Кафедра фізики, Федеральний університет наук про здоров'я, Отукпо, штат Бенуе, Нігерія
[b]Кафедра фізики, Федеральний технологічний університет, Мінна, штат Нігер, Нігерія
[c]Центр ядерних технологій, Комісія з атомної енергії Нігерії, Абуджа, Нігерія
[d]Кафедра фізики, Університет Бінгема, штат Насарава, Нігерія
[e]Кафедра фізики, Університет штату Бенуе, штат Бенуе, Нігерія
[f]Кафедра фізики, Державний університет Насарава, штат Насарава, Нігерія
[g]Відділ електротехніки/електронної інженерії Нільського університету Нігерії
[h]Факультет фізики, Університет Нігерії Ннсукка, штат Енугу, Нігерія
[i]Факультет фізики, Університет штату Ріверс, Порт-Гаркорт, штат Ріверс, Нігерія
[j]Африканський центр передового досвіду в галузі енергетики майбутнього та електрохімічних систем, Федеральний технологічний університет, Оверрі, штат Імо, Нігерія

Перовскітні сонячні батареї (PSC) привернули велику увагу завдяки своїй високій ефективності та низькій вартості. У цій дослідницькій роботі сонячний елемент на основі йодиду метиламонію олова ($CH_3NH_3SnI_3$) моделювався за допомогою інструменту моделювання одновимірної ємності сонячного елемента (SCAPS-1D). Інструмент SCAPS-1D заснований на рівняннях Пуассона та напівпровідників. Після ретельного дослідження початковий пристрій має наступні параметри; Ефективність перетворення потужності (PCE) = 15,315%, коефіцієнт заповнення (FF) = 64,580%, щільність струму (Jsc) = 29,152 мА/см^2 і напруга холостого ходу (Voc) = 0,813 В. Досліджено вплив товщини абсорбера та ETL систематично. На продуктивність змодельованого пристрою суттєво вплинула товщина абсорбера та ETL. Оптимізована товщина поглинача становила 0,5 мкм, а товщина ETL становила 0,02 мкм, що призвело до оптимізованого PCE 15,411%, FF 63,525%, Jsc 29,812 мА/см^2 і Voc 0,814 В. Крім того, вплив температури на оптимізований пристрій було оцінено та виявлено, що це впливає на продуктивність пристрою. Ця модель показує перспективу $CH_3NH_3SnI_3$ як перовскітного матеріалу для виробництва нетоксичних екологічно чистих сонячних елементів з високою ефективністю.

Ключові слова: *перовскітний сонячний елемент; SCAPS-1D; $CH_3NH_3SnI_3$; фотоелектричний*